International Journal of Sustainable Energy and Environmental Research
2026 Vol. 15, No. 2 pp. 1-17
ISSN(e): 2306-6253
ISSN(p): 2312-5764
DOI: 10.18488/13.v15i2.5047
© 2026 Conscientia Beam. All Rights Reserved.

Synthesis of multilayer graphene from plastic waste for the modification of battery cathode material

Md. Ramjan Ali[1]
Md. Osman Ali[2+]
Md. Erfanul Hasan Sakib[3]
Nieom Biswas[4]
Aneek Barua[5]
Samim Mahbub[6]
Salman Ali[7]
Sumon Roy[8]
Md Masud Rana[9]
Md. Akibul Islam[10]
Ekramul Islam[11]

[1,2,3,4,5,6,7,8,9,10,11]*Department of Mechanical Engineering, Dhaka University of Engineering and Technology, Gazipur, Gazipur-1707, Bangladesh.*
[1]*Email: ramjan@duet.ac.bd*
[2]*Email: osman@duet.ac.bd*
[3]*Email: erfanulhasansakibduet@gmail.com*
[4]*Email: nieombiswas@gmail.com*
[5]*Email: baruaanik47@gmail.com*
[6]*Email: bdshamimmahbub@gmail.com*
[7]*Email: salman.shatkania@gmail.com*
[8]*Email: srsumon288@gmail.com*
[9]*Email: mrdeeptoduet@gmail.com*
[10]*Email: akib@duet.ac.bd*
[11]*Email: mdikramislam210@gmail.com*



(+ Corresponding author)

Article History
Received: 6 May 2026
Revised: 15 June 2026
Accepted: 3 July 2026
Published: 17 July 2026

Keywords
Alumina (Al_2O_3)
Battery cathode
Energy storage
Graphene
Two-step pyrolysis
Waste plastics.

ABSTRACT

The widespread production and use of plastics have raised environmental concerns due to their non-biodegradable nature. Effective waste management and conversion of waste into value-added products can be a sustainable solution. This study converts waste plastic into graphene to modify the Nickel–Manganese–Cobalt oxide (NMC) cathode with alumina (Al_2O_3). The Al_2O_3 percentage was varied from 1.0 to 2.0%, with a constant graphene percentage of 6.0%. Extensive analysis using Raman, XRD, FESEM, FTIR, UV-vis, and TGA demonstrated the successful transformation of waste plastic into multilayered graphene with graphitic stacking. The Raman analysis showed an ID/IG ratio of 1.07, which suggests edge defects and limited crystalline domain size, and an I2D/IG ratio less than 1.0 indicates the presence of multilayer graphene nanosheets. A UV absorbance peak at 295 nm in graphene highlights its suitability for optical applications. The thermal stability of graphene up to 600 °C makes it ideal for high-temperature applications. Nanosheet boundaries appear as irregular, overlapping lines or ridges on the surface and are stacked randomly with a crumpled morphology. SEM, FTIR, and XRD characterization of the NMC cathode with 2.0% Al_2O_3 and 6.0% showed better surface quality than other compositions. The charging test results for this cathode show good compatibility with electrodes and a stable interphase. Overall, the results suggest that rapid, large-scale synthesis of high-quality graphene from waste plastics offers significant potential for sustainable graphene production and is viable for future battery research.

Contribution/Originality: This study contributes by focusing on the conversion of plastic waste into graphene and its implementation in battery cathode materials, which can be promising for increasing cathode stability, whereas most existing studies have focused on converting plastic waste into carbon materials only.

© 2026 Conscientia Beam. All Rights Reserved.

1. INTRODUCTION

Human activity nowadays is more dependent on energy due to economic growth and urbanization, and this energy is obtained mainly from finite fossil fuels, which exacerbate environmental problems (Ali et al., 2026). Energy storage has become feasible in modern times, and batteries are among the most effective and popular devices for this use (Chojaa et al., 2023; Elessawy, Rafea, Roushdy, Youssef, & Gouda, 2023). In recent years, batteries have become an ineluctable part due to advancements in electric and hybrid vehicles, as well as electronic appliances like laptops, remotes, mobile phones, and drones (Ali et al., 2023). Among several batteries, the lithium-ion battery is the most promising energy source owing to its unprecedented stability in performance, better stability, and cycle life, along with its unique electrochemical characteristics (Saffanah, Avis, Widiyandari, Jumari, & Purwanto, 2025; Tunca et al., 2024). To mitigate high energy storage demand, research is ongoing on lithium-ion batteries regarding the modification of energy density, cycle life, and safety (Blázquez-Moreno et al., 2025; Kumarov et al., 2025; Yerkinbekova et al., 2025). This research focuses on one of the fundamental battery components, such as the anode, cathode, electrolyte, or separator. The oxidation/reduction (redox) reactions that occur between the battery electrodes largely depend on the amount of active material present in each electrode (Jekal et al., 2024).

Extensive research is ongoing on several battery cathode materials, such as Nickel Manganese Cobalt (NMC), Lithium Manganese Spinel (LMO), Lithium Nickel Manganese Spinel (LNMO), and Lithium Iron Phosphate (LFP) (Argañaraz et al., 2025). Among these cathode materials, the NMC cathode has received more attention due to its high nickel content, capacity per unit mass, extreme current stability, better volumetric density, and long cycle life (Kumarov et al., 2025). However, the direct application of NMC and its performance are restricted because of its high lithium content, fast capacity fall, and poor electrical conductivity under specific conditions (Ahaliabadeh, Kong, Fedorovskaya, & Kallio, 2022; Llanos et al., 2024). To address this, various modifications to the NMC cathode have been investigated, including the use of nanoscale particles and the incorporation of conductive materials to improve electron transport (Park, Sherrell, Xie, & Ellis, 2024; Zhang et al., 2024).

Recent developments in nanotechnology have increased research by helping the use of nanoparticles as reinforcement. The most commonly used nanoparticles are titanium dioxide (TiO_2), silicon carbide (SiC), graphene, graphene oxide (GO), aluminum oxide (Al_2O_3), zinc oxide (ZnO), zirconium dioxide (ZrO_2), carbon nanostructures (CNs), multi-walled carbon nanotubes (MWNTs), and copper nanoparticles. Among these, graphene is the best-suited nanomaterial due to its unique electrical conductivity and large surface area (Chen et al., 2020). Recently, two-dimensional (2D) transition-metal layered materials have become critical for sensing, catalysis, and energy storage, particularly since the discovery of monolayer graphene (Fang et al., 2015). Graphene, a single layer of carbon atoms organized in a hexagonal lattice, has exceptional properties that make it a viable material for applications in energy, electronics, and sensors (Balqis et al., 2023). Since 2004, graphene has been considered one of the most significant scientific and technological breakthroughs (Ojha, Samriti, Thakur, & Prakash, 2023). Graphene has exceptional mechanical (Lee, Wei, Kysar, & Hone, 2008), electrical (Geim & Novoselov, 2007), and thermal (Balandin et al., 2008) properties, which make it useful in a wide range of applications, such as biomedical (Derakhshi et al., 2022), energy storage (Salahdin et al., 2022), electronics (Wu, Lin, Moss, Loh, & Jia, 2023), coatings (Malayeri, Koohestani, & Tajally, 2023), sensors (Liu, Bao, & Wang, 2022), composites (Tarhini & Tehrani-Bagha, 2023), solar cells (Velasco, Díez-Pascual, & Capilla, 2022), batteries fuel cell (Okonkwo et al., 2022), drug delivery (Itoo et al., 2022), water purification (Wu et al., 2022), and so on. The most common synthesized methods for graphene are mechanical exfoliation (Whitener & Sheehan, 2014), chemical vapor deposition (CVD) (Saeed, Alshammari, Majeed, & Al-Nasrallah, 2020), epitaxial growth on silicon carbide (SiC) (Huang, Chen, Wee, & Chen, 2014), chemical reduction (Jiang et al., 2013), exfoliation of graphite through solution oxidation and sonication (Lavin-Lopez, Valverde, Sanchez-Silva, & Romero, 2016), and so on. However, traditional processes for producing expensive, structurally flawed graphene, such as mechanical exfoliation and chemical vapor deposition, are costly, time-consuming, and often

© 2026 Conscientia Beam. All Rights Reserved.

yield only small amounts of the material. The introduction of a cost-effective graphene production technology will significantly accelerate its industrialization.

Plastics are omnipresent in daily life due to their lightweight and versatile nature (Jahandari, 2023; Ramos et al., 2023). However, their increasing use has led to significant environmental issues. Waste plastic from careless disposal harms ecosystems, wildlife, and human health (Dey, Veerendra, Babu, Manoj, & Nagarjuna, 2024). The circular economy depends on sustainable production and consumption by promoting the reuse of materials. Despite this, challenges remain in effectively recycling high-carbon materials like plastic waste due to degradation difficulties and limited disposal options. Waste plastics, made of carbon-based polymers, can be transformed into graphene through various methods (Bharti & Sharma, 2021; Pandey et al., 2019; Vieira, Ribeiro, De Tuesta, Gomes, & Silva, 2022). This approach addresses environmental issues related to solid waste while enabling the extraction of valuable compounds. Studies show that waste plastics such as polypropylene (PP), polystyrene (PS), polyethylene (PE), and polyethylene terephthalate (PET) are effective precursors for producing carbon nanomaterials (CNMs), including carbon nanotubes, carbon nanofibers (CNFs), carbon spheres, and graphene (Belbessai, Benyoussef, Gitzhofer, & Abatzoglou, 2022; Dhali, Karakoti, Dandapat, & Sahoo, 2023; Ren et al., 2022; Tan, Ahmad, Da Oh, & Low, 2023).

Although plastic-derived graphene has been studied previously, challenges remain in achieving scalable production methods and applying it to functional electrochemical systems. In this work, a two-step pyrolysis process combined with mechanical processing and ultrasonic exfoliation was used to produce multilayer graphene from plastic waste. The synthesized multilayer graphene was incorporated into NMC cathodes with the addition of Al_2O_3 to investigate the combined effect on surface morphology, structural characteristics, and electrochemical performance.

2. MATERIALS AND METHODOLOGY

2.1. Materials

NMC powder was manually extracted from a Lithium Nickel Manganese Cobalt Oxide battery (Manufacturer: LG Chem, now LG Energy Solution). Aluminum Oxide (Al_2O_3) was collected from Loba Chemie Pvt. Ltd. (India) for its chemical stability and thermal resistance, which protect the cathode surface and enhance stability. Polyacrylic Acid (PAA) $(C_3H_4O_2)_n$ from Sigma-Aldrich (Merck) was used as a binder in electrode materials, providing chemical stability. Graphene was synthesized from plastic waste using a two-step pyrolysis process. Aluminum foil with a thickness of 12–20 μm was obtained from Walton Digi-Tech, Bangladesh, for use as a battery cathode.

2.2. Synthesis of Graphene from Plastic Waste

Approximately 50 kg of polyethylene terephthalate (PET) bottles were gathered from both the local neighborhood and the municipality. It was then finely shredded into small, flake-like pieces using a shredder. The plastic pieces were subsequently washed with a soap solution to remove oily and greasy contaminants. Subsequently, the plastic fragments were dried outdoors. Following the completion of the washing and drying procedures, the waste plastics were subjected to slow pyrolysis in a controlled environment under an inert nitrogen (N_2) atmosphere at a flow rate of 20 mL/min at 400 °C. A charred residue of amorphous carbon was produced during slow pyrolysis and was obtained after separating all petroleum-based products. A ball mill was used to grind the collected residue into a fine powder. After that, this fine powder was thoroughly mixed with 5 wt.% Bentonite nano clay using a sample mixing machine.

Subsequently, the sample mixture was rapidly heated in the secondary furnace under a nitrogen (N_2) flow rate of 30 mL/min at 750 °C, forming a black-colored structure composed of graphene flakes. To transform a few layers of high-quality graphene, the collected flakes were ultrasonicated in acetone for at least 2 hours. The sonicated solution was centrifuged at a speed of 3000 rpm for an hour. Consequently, flakes settled to the bottom of the test tube, whereas the solution remained dispersed, indicating the presence of high-quality graphene. The systematic process of graphene synthesis from waste plastic is shown in Figure 1.

© 2026 Conscientia Beam. All Rights Reserved.

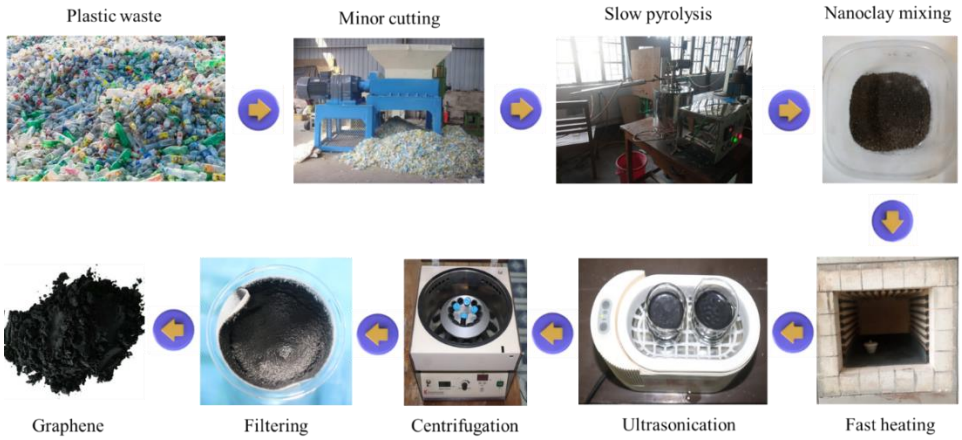


Figure 1. Ultrasonic-assisted pyrolysis process of graphene synthesis from waste plastics.

2.3. Preparation of NMC Cathode

Initially, the NMC battery cell was carefully cut open in a controlled environment to prevent short-circuiting and exposure to hazardous components. The cathode foil was separated from the cell structure using non-metallic tweezers. After separation, the cathode foil was cleaned, and the NMC (Nickel-Manganese-Cobalt oxide) active material was removed by scraping it from the aluminium current collector. The extracted NMC material was collected and stored in an airtight container for further use. In the next step, analytical-grade aluminium oxide (Al_2O_3) and graphene powders were used as the composite matrix and conductive additive, respectively. Three samples were prepared using the same general procedure, with differing compositions. For sample preparation, NMC powder, Al_2O_3, and graphene were weighed precisely using a digital weighing balance (Model: PS. P3.610). The measured powders were thoroughly mixed using a mortar and pestle to achieve uniform blending. The mixture was then dried in an oven at a moderate temperature to remove any moisture. After drying, an appropriate quantity of polyacrylic acid (PAA) binder was added to the mixture to improve adhesion between the active material and the aluminium foil, followed by ultrasonication for 10 minutes to ensure homogeneous dispersion of all components. After sonication, the prepared solvent was uniformly coated onto previously cut small aluminium foil substrates. The coated foils were left in the open air and later placed in an oven to allow complete drying at room temperature. These prepared electrode samples were then stored in a desiccator to prevent moisture absorption before subsequent physical and structural characterization. The whole process is demonstrated in Figure 2.

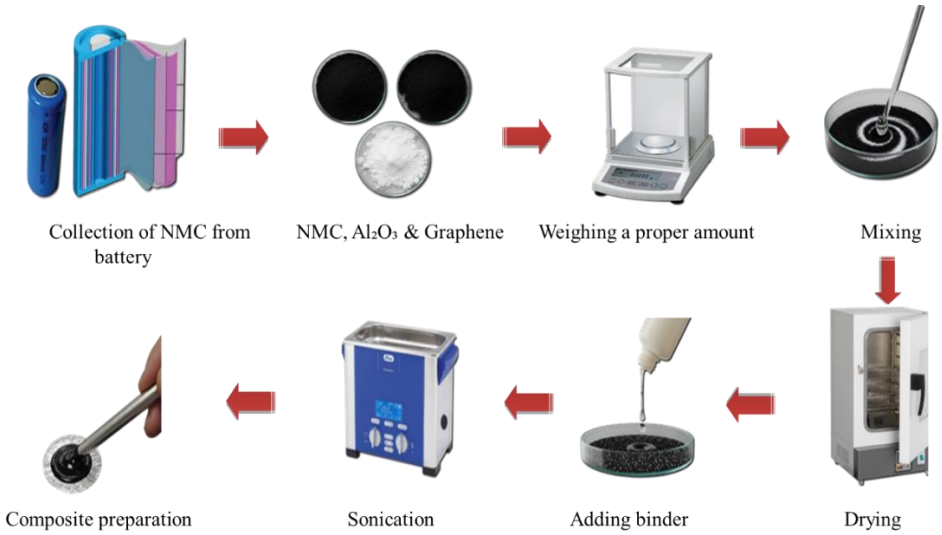


Figure 2. Fabrication of the NMC samples.

© 2026 Conscientia Beam. All Rights Reserved.

2.4. Surface Morphology Characterization

A vacuum cleaner combined field emission scanning electron microscope (FESEM) (JEOL, JSM 7610F) was used to analyze the surface morphologies of graphene, while a scanning electron microscope (Hitachi SU1510) was used for cathodes. For SEM analysis, samples were prepared as solid specimens measuring 2 mm × 2 mm. The setup included a copper plate wrapped in carbon tape, on which the samples were placed, followed by a platinum coating.

2.5. Phase Structure Analysis

X-ray diffraction measurements were conducted on the materials using XRD, and the diffraction intensities were recorded over a range of diffraction angles (2θ). X-ray diffraction was employed to determine the crystallinity of the composite materials. The investigation of structural properties used a Bruker D8 Advance X-ray diffractometer (XRD) combined with a monochromatic Cu Kα radiation source (λ = 1.5418 Å) and a mono Vista CRS+ Raman spectrometer. A Bruker D8 Advance (or D8 Discover) (Manufacturer: Bruker AXS GmbH) device was used to investigate the structural properties of the NMC cathode at room temperature. Data were collected at a scanning rate of 3°/min with an interval of 0.05° over the 2θ range of 10-80°.

2.6. Chemical Functional Group Analysis

Infrared light was used to scan the samples and identify the functional groups using FTIR analysis. The functional properties of synthesized graphene were investigated using UV-Vis spectroscopy (UV 3600 Shimadzu, Japan) and Fourier transform infrared spectroscopy (FTIR) (Perkin Elmer, USA). A Thermo Scientific Nicolet iS5 FTIR spectrometer was employed to obtain the FTIR spectra of the fabricated samples. When preparing the samples as thin films on glass plates, the wavelength range was adjusted from 450 to 4000 cm^{-1}.

2.7. Thermogravimetric Analysis

Thermal Gravimetric Analysis (TGA) was employed to evaluate the thermal stability and temperature-dependent behavior of the synthesized graphene, providing insights into thermal decomposition, absorption, desorption, and oxidation- or reduction-related phase transitions. The thermal stability of the synthesized graphene was investigated using a thermogravimetric analyzer (TGA) (SDT 650).

2.8. Charging Test Analysis

A charge-discharge cycle test is a valuable method to evaluate battery performance, cycle life, and stability. The charging performance of the fabricated cell was assessed using a LAND battery testing system (Model: CT2001A). In this experiment, the cathode material, prepared by combining NMC (Nickel Manganese Cobalt) with 6% Graphene and 2% Al_2O_3 (i.e., sample-1), was tested, while the anode material was sourced from the market, composed of a mixture of Graphite, Silicon Carbide (SiC), Tin (Sn), and Cobalt (Co). During the electrochemical charging tests, a 1 M lithium sulfate (Li_2SO_4) aqueous solution was used as the electrolyte. A 20 μm polypropylene/polyethylene (PP/PE) microporous membrane served as the separator, and the cells were assembled in a CR2032 coin cell configuration, with the working and counter electrodes stacked with the separator in between and sealed in a stainless-steel coin cell case.

3. RESULTS AND DISCUSSION

3.1. Characterization of Synthesized Graphene

Fundamental physical characterization techniques, including SEM, FTIR, and XRD, confirmed the successful synthesis of graphene. Conversely, TGA analysis ensures the thermal stability of the synthesized graphene.

© 2026 Conscientia Beam. All Rights Reserved.

3.1.1. Surface Morphology Characterization of Synthesized Graphene

The growth and structure of graphene were examined using field-emission scanning electron microscopy (FESEM), as shown in Figure 3. The resulting graphene sheets exhibited a crumpled morphology, with layers stacked randomly (Garg et al., 2022). The images of the graphene nanosheets clearly revealed edge flaws at multiple locations. The boundaries can be seen as irregular, overlapping lines or ridges on the surface of the graphene sheet (Biró & Lambin, 2013). The findings suggest that the nucleation density must be controlled to produce good-quality graphene nanosheets, which may be achieved by controlling the pyrolysis temperature. Studies indicate that slow temperature increases up to 400 °C result in low carbon radical rates and low nucleation densities. Conversely, rapid heating to 750 °C causes graphene nanosheets to merge, forming more prominent cluster-type structures.

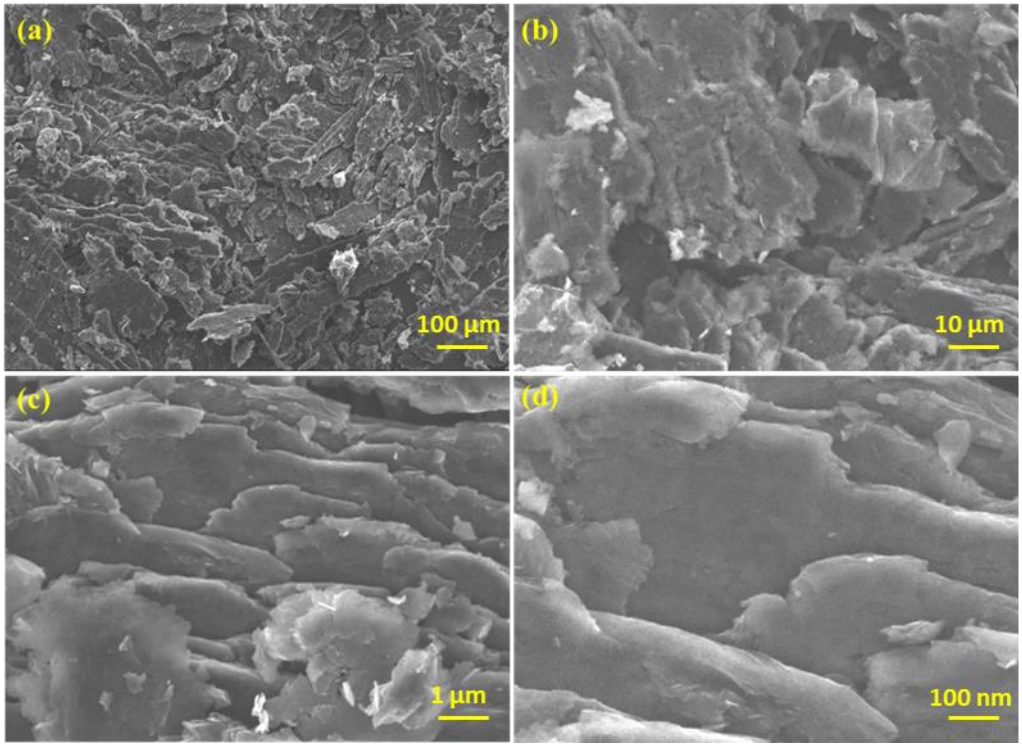


Figure 3. FESEM images of graphene at (a) 100 µm, (b) 10 µm, (c) 1µm, and (d) 100 nm magnification.

3.1.2. Phase Structure Analysis of Synthesized Graphene

The XRD investigation of the synthesized graphene nanosheets is shown in Figure 4a. The characteristic peaks of graphene are visible in the XRD spectrum as diffraction peaks of (002) and (004) at $2\theta \approx 26.94°$ and 55°, respectively. The XRD peaks broaden as the crystallite size decreases from bulk to nanoscale dimensions, indicating the bulk homogeneity of the graphene (Zhou et al., 2013). Table 1 shows the full width at half maximum (FWHM), interplanar spacing (d), and the coherent stacking height (Lc) estimated from the (002) peak. The FWHM is calculated by a Gaussian fit using OriginLab. The Lc was calculated using the Scherrer equation applied to the (002) reflection, while the interlayer distance (d) is calculated using Bragg's equation.

Scherrer's Equation:

$$L = \frac{k\,\lambda}{\beta \cos\theta} \qquad (1)$$

Where λ is the X-ray wavelength, with a value of 0.15406 Å, β is FWHM in radians, θ is the half diffraction angle in radians, and k is a constant related to crystallite shape, assumed to be 0.9.

Bragg's equation:

$$d = \frac{n\lambda}{2\sin\theta} \qquad (2)$$

© 2026 Conscientia Beam. All Rights Reserved.

According to Table 1, the values of FWHM, stacking height (Lc), and interplanar spacing (d) at $2\theta = 26.94°$ are 0.645°, 11.78 nm, and 0.331 nm, respectively. The relatively narrow FWHM indicates ordered graphitic-layer stacking. The calculated interlayer spacing (0.331 nm), close to that of crystalline graphite (0.335 nm), confirms the formation of a multilayered graphitic structure. The estimated stacking height (Lc) of 11.78 nm, obtained from the (002) reflection using the Scherrer equation, suggests the development of stacked graphitic domains with moderate crystalline ordering (Ivanov, Maksimova, Kamaev, Malakho, & Avdeev, 2018). These results demonstrate that pyrolysis of plastic waste facilitates the formation of multilayer graphene with graphitic characteristics.

The structural properties of graphene nanosheets were demonstrated using Raman spectroscopy, as shown in Figure 4b and Table 1. The spectrum generated from graphene nanosheets displays two discernible bands: the D-band, observed at a wavenumber of 1480 cm^{-1}, which arises from the stretching of sp3 carbons, and the G band, observed at 1570 cm^{-1}, originating from the stretching of sp2 carbons (Ayiania, Weiss-Hortala, Smith, McEwen, & Garcia-Perez, 2020). The observed IG/ID ratio of 0.93 indicates the presence of edge defects in the graphene structure, reflecting a smaller size of the graphene sheet (Tang, Guoxin, & Gao, 2010). Additionally, there is a small 2D band at 2710 cm^{-1}. The relationship between the intensity of the 2D and G peaks (I2D/IG) is influenced by the number of layers in graphene (Kang et al., 2023; Kim et al., 2019; Kumar et al., 2014). The I2D/IG ratio is approximately 2-3 for monolayer graphene, greater than 1 but less than 2 for bilayer graphene, and less than 1 for multilayer graphene. That is, the I2D/IG ratio reflects the layers of graphene, and less than 1.0 indicates the presence of multilayers of graphene nanosheets (Lan et al., 2018). The produced graphene has an I2D/IG ratio of 0.3, below 1, suggesting the presence of multilayer graphene.

The structural defects observed in the synthesized multilayer graphene can be attributed to several aspects of the synthesis process. The initial slow pyrolysis at 400 °C produces amorphous carbon with limited structural ordering. Although secondary heat treatment at 750 °C promotes graphitization, this temperature is lower than that typically required for highly crystalline graphite formation. Furthermore, the synthesis was performed without the use of metal catalysts, which limits long-range crystalline reconstruction and results in defect-rich graphitic domains. Mechanical ball milling and ultrasonic exfoliation may also introduce edge defects and reduce crystalline domain size. Additionally, minor surface oxidation during processing and handling cannot be excluded. These factors contribute to the defect-rich multilayer graphene structure observed in the Raman analysis.

Table 1. Structural parameters of the graphene nanosheets.

Peak (2θ)°	FWHM (degree)	Inter-planar spacing, d (nm)	Stacking height, Lc (nm)	Peak position (cm^{-1})			Peak intensity			Peak intensity ratio	
				D	G	2D	I_D	I_G	I_{2D}	I_D/I_G	I_{2D}/I_G
26.94	0.645	0.331	11.78	1480	1570	2710	1770	1645	490	1.07	0.29

3.1.3. Chemical Functional Group Analysis of Synthesized Graphene

The FTIR spectrum of the graphene nanosheets is shown in Figure 4c. This spectrum includes various functional groups, such as hydroxyl (O-H), cyclic nitroxides (N-O), and carbonyl (O=C=O), due to the slight oxidation of graphene. The presence of OH and/or COOH functional groups in graphene is indicated by medium O-H stretching vibrations at 3785 cm^{-1}. Additionally, significant O=C=O stretching vibrations were visible in the FTIR spectra of graphene nanosheets at 2360 cm^{-1} and comparatively weak N-O stretching vibrations at 1598 cm^{-1} (Kumar, Gambarelli, Duclairoir, Bidan, & Dubois, 2013). The UV-Vis spectrum is shown in Figure 4d. Notably, the size dependence of UV absorbance in the 220-500 nm range is remarkable (Saleem, Haneef, & Abbasi, 2018). The absorption peak of graphene nanosheets is at 295 nm, demonstrating a strong response of the graphene nanosheets across the UV spectrum.

© 2026 Conscientia Beam. All Rights Reserved.

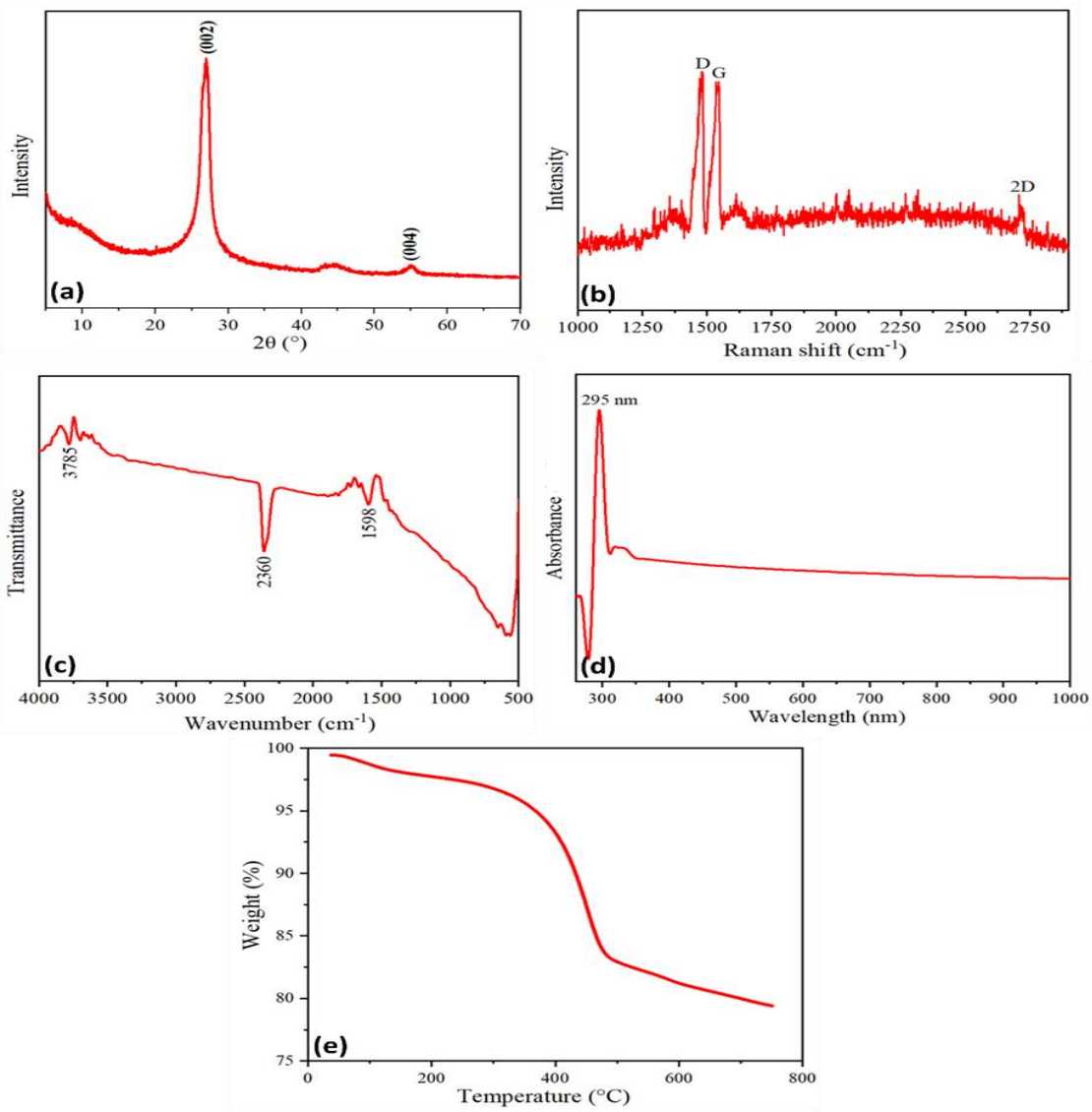


Figure 4. Characterization of graphene by (a) XRD, (b) Raman, (c) FTIR, (d) UV-vis, and (e) TGA analysis of graphene nanosheets.

3.1.4. Thermogravimetric Analysis

Thermogravimetric analysis (TGA) was employed to investigate the thermal stability or degradation of the synthesized graphene. Figure 4e illustrates the thermal decomposition process of the synthesized graphene, which occurs in two distinct stages. A slight decrease in mass (approximately 3%) was observed at approximately 250 °C, attributable to the desorption of water molecules adsorbed on the specimen. A notable 15% reduction in weight was observed in the temperature range of 250 °C to 600 °C, attributable to the decomposition of oxygen-containing functional groups. Over the entire temperature range (ambient to 750 °C), it loses only 20% of its weight, indicating the thermal stability of the synthesized graphene (Soltani & Lee, 2017).

3.2. NMC-Alumina-Graphene Cathode

The NMC cathode composite was fabricated on a thin Al_2O_3 layer that serves as a protective coating to enhance stability. Graphene, as a conductive additive, may improve the electronic conductivity, structural integrity, and overall electrochemical performance of the cathode. Table 2 shows the composition details of each fabricated sample.

© 2026 Conscientia Beam. All Rights Reserved.

Table 2. Details about the composition of the fabrication samples.

Sample No.	Composition	Weight of the composition		
		NMC (gm)	Al_2O_3 (gm)	Graphene (gm)
S1	NMC+2%Al_2O_3+6% Graphene	0.98	0.02	0.06
S2	NMC+1.5%Al_2O_3+6% Graphene	0.985	0.015	0.06
S3	NMC+1%Al_2O_3+6% Graphene	0.99	0.01	0.06

To determine whether the NMC composites were successfully formed, fundamental physical characterization techniques, including SEM, FTIR, and XRD, were employed.

3.2.1. Surface Morphology Characterization of the Fabricated Cathode

The Scanning Electron Microscopy (SEM) was used to determine surface morphology, microstructure, bonding, porosity, and particle distribution of composite materials at very high magnifications.

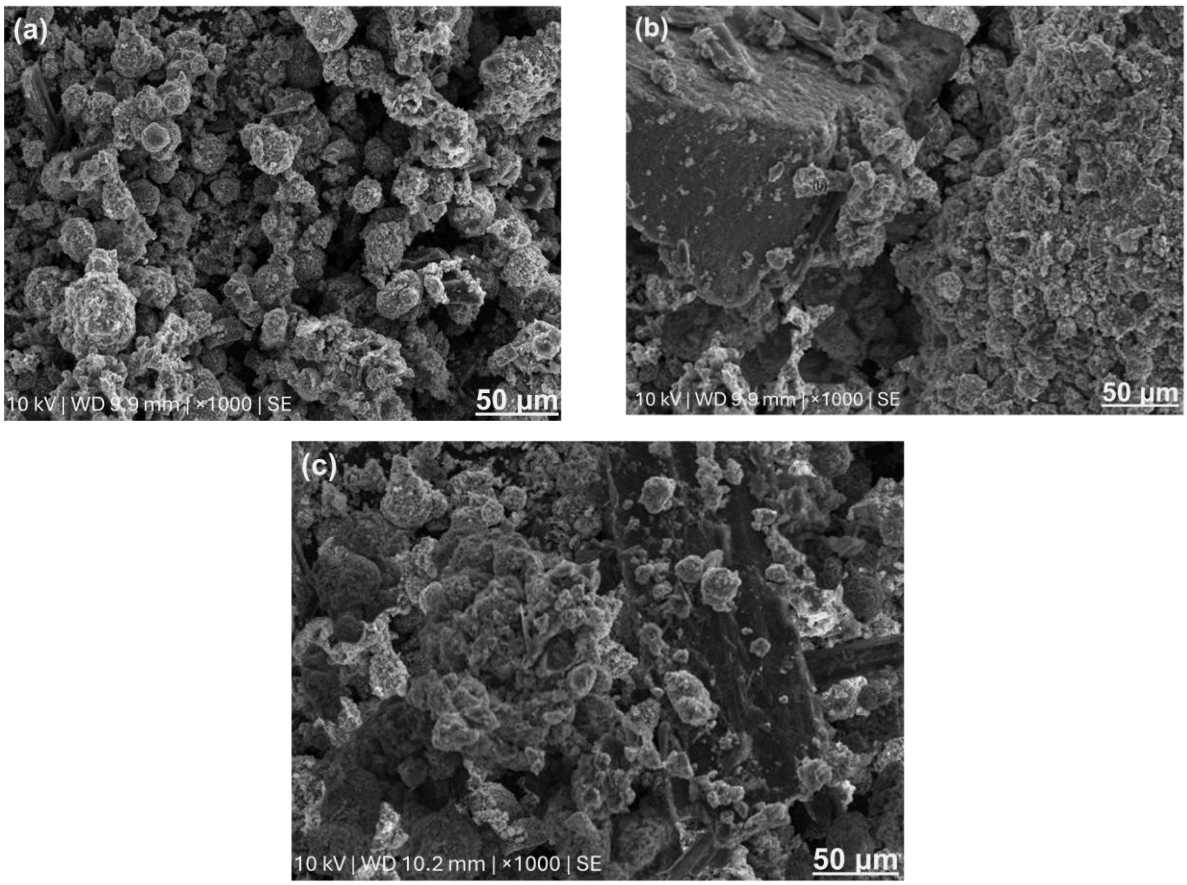


Figure 5. SEM micrographs of (a) NMC+2%Al_2O_3+6% Graphene, (b) NMC+1.5%Al_2O_3+6% Graphene, and (c) NMC+1%Al_2O_3+6% Graphene.

Figure 5 represents the SEM micrographs of the NMC with graphene - Al_2O_3 coated composite, captured with a scale bar of 50 µm. All SEM micrographs exhibited a nearly regular shape. As shown in Figure 5(a), the NMC cathode with 2% Al_2O_3 and 6% Graphene exhibits denser SEM micrographs with rougher surface textures. This indicates strong interactions and adhesion between the constituent materials. This proper dispersion is crucial to enhance surface stability, reduce direct electrolyte contact, and contain unnecessary particle growth during cycling (Setyawati et al., 2024). The rough, granular surface indicates that the composites have effectively improved the NMC particle layer. The other two micrographs in Figure 5. (b) and (c), however, displayed a nonhomogeneous but continuous

© 2026 Conscientia Beam. All Rights Reserved.

surface layer micrograph due to the insufficient proportion of Al_2O_3. These SEM micrographs exhibit relatively heterogeneous particle shapes and sizes, with high surface texture. Some particles are stacked and form cluster-like shapes. In all the micrographs, the NMC grains are surrounded by thin, interconnected graphene layers. No distinct Al_2O_3 particles can be observed on the surface of the NMC due to the nanoscale and amorphous nature of alumina, indicating that the particles are dispersed uniformly on the surface (Loghavi, Babaiee, & Eqra, 2023).

Overall, the SEM results confirm that surface modification and composite formation were successfully achieved, and the 2% Al_2O_3 sample displays the most uniformly coated surface, indicating optimal integration of graphene and Al_2O_3 that may improve stability and electrical conductivity crucial for high-performance battery cathodes.

3.2.2. Chemical Functional Group Analysis of the Fabricated Cathode

Fourier Transform Infrared Spectroscopy (FTIR) was used to analyze the chemical structure and functional groups of NMC composites with Al_2O_3 and graphene.

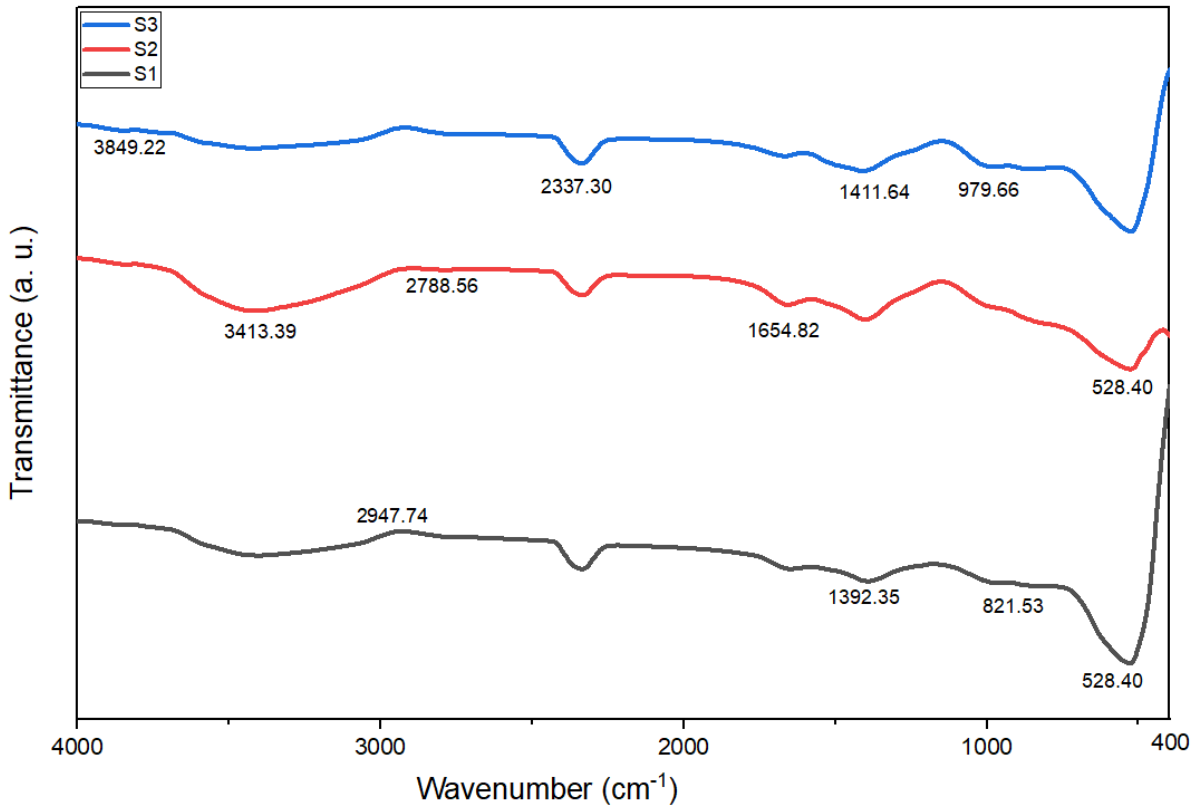


Figure 6. FTIR patterns of the fabricated NMC-graphene cathodes.

The FTIR patterns of the fabricated NMC cathode samples modified with a graphene–Al_2O_3 composites are shown in Figure 6. The three patterns, with Al_2O_3 concentrations of 1%, 1.5%, and 2% and a constant 6% graphene, show how varying the Al_2O_3 content affects the surface chemistry and bonding structure of the NMC composite. However, the synthesized NMC composites exhibited very similar overall FTIR patterns, except for slight variations in wavenumbers and transmittance percentages, indicating constant compositions across the samples. As can be seen from the transmittance (%) FTIR patterns, a small band at ~3849 cm^{-1} is attributed to free surface O–H stretching vibrations, possibly due to the isolation of hydroxyl groups on alumina. A broad and intense absorption band centered at 3400 cm^{-1} indicates the O–H stretching vibration, originating from surface hydroxyl groups or adsorbed moisture. Bands observed in the 2788–2947 cm^{-1} region are attributed to aliphatic C–H stretching vibrations arising from organic binder components and residual solvents. The peak at ~2333–2337 cm^{-1} is due to CO_2 stretching and does not affect chemical bonding. The broader peaks at ~1646–1667 cm^{-1} are assigned to C=C stretching. The presence of

© 2026 Conscientia Beam. All Rights Reserved.

these spectra confirms the presence of multilayer graphene structures (Ferrari et al., 2006). A band observed at ~1400 cm^{-1} is assigned to the asymmetric stretching vibration of carbonate species, likely arising from surface Li_2CO_3. This band is attributed to surface reactions with ambient CO_2. Strong metal–oxide vibrations are observed at ~980 cm^{-1}, ~837 cm^{-1}, and ~528 cm^{-1}, characteristic of metal-oxygen stretching vibrations (Ni–O, Co–O, Mn–O) in layered oxide frameworks, which are essential to the spinel or layered oxide structure of NMC-based materials (Sanad, Meselhy, El-Boraey, & Toghan, 2023). The strength of these peaks indicates robust bonding and high crystallinity of the metal oxide lattice. This confirms the presence of metal-oxide links within the structure. These features verify that Al_2O_3 is chemically bonded to the NMC surface rather than merely being physically mixed.

FTIR analysis reveals effective integration of Al_2O_3 and graphene on the NMC surface, with variations in absorption bands indicating structural and chemical changes linked to Al_2O_3 content. These modifications enhance chemical stability and compatibility, demonstrating successful surface modification and improved electrochemical performance.

3.2.3. Phase Structure Analysis of the Fabricated Cathode

X-ray diffraction (XRD) is primarily used to determine the phase structure, specifically whether the fabricated NMC cathodes are crystalline, semicrystalline, or amorphous.

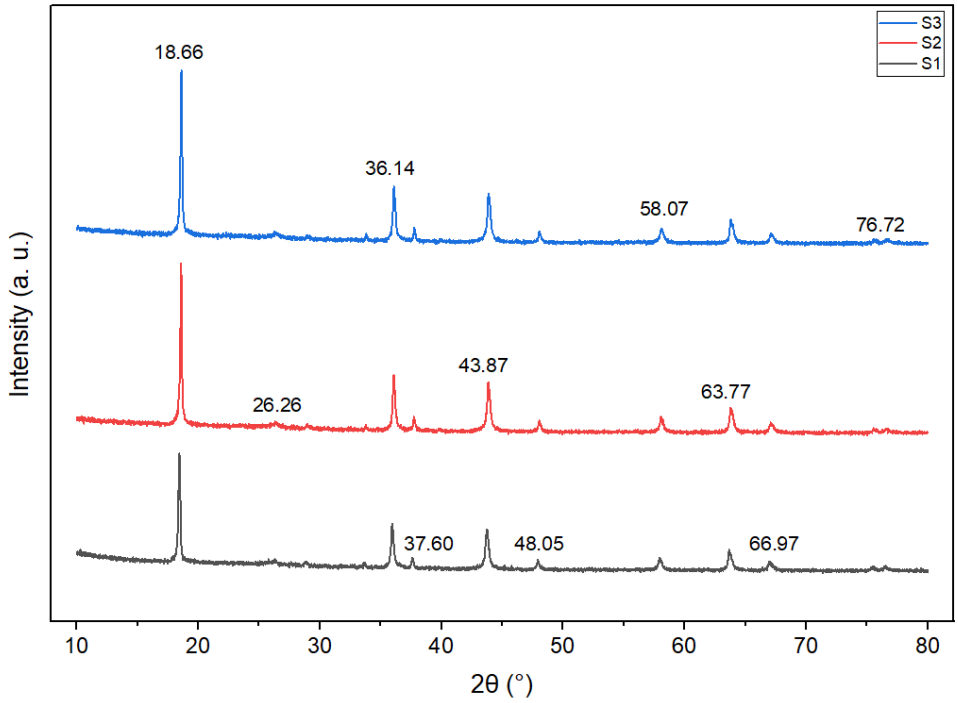


Figure 7. XRD spectra of the fabricated NMC cathodes.

The X-ray diffraction (XRD) pattern of the fabricated NMC cathode samples modified with graphene–Al_2O_3 composites is shown in Figure 7. The synthesized NMC composites exhibited very similar overall XRD spectra, except for slight variations in 2θ and intensity values, indicating consistent compositions among the samples. Most peaks appeared between 15 and 80°. The most prominent sharp peak was observed at 2θ = 18.0–19.0°. Other major peaks were found around 2θ values of 26, 36–37, 43, 48, 58, 64, 67, and 77°. These sharp and associated diffraction peaks were consistent with the layered hexagonal α-$NaFeO_2$ structure in the $R\bar{3}m$ space group. The peaks at ~36–37° and 64° confirm the presence of a well-ordered layered structure (Ma, Cui, Gan, Ma, & Liang, 2018). Peaks near 2θ ~ 18.0–19.0° and 43–48° indicate proper crystallinity of the NMC-graphene cathode (Ronduda et al., 2020). The peak at 26° suggests that graphene layers are farther apart, with increased interlayer spacing (Chen et al., 2022).

© 2026 Conscientia Beam. All Rights Reserved.

With increasing graphene content, the peak height tends to increase. Based on these results, it can be said that the surface treatment of the NMC cathode with graphene affects its crystal structure of the cathode (Güngör, Güler, Çoban, Güler, & Akbulut, 2018). Al2O3 is structurally stable and does not chemically bond with the NMC structure, as evidenced by weak reflections in the XRD pattern and no significant interaction with the NMC lattice. This supports prior research indicating that Al2O3-coated NMC cathodes create a thin, X-ray-amorphous protective layer while maintaining the bulk R-3m structure of NMC (Chen et al., 2025; Han et al., 2017; Mohanty et al., 2016).

3.2.4. Charging Test Analysis

Figure 8 shows the constant-current (1.0 mA) charging of the fabricated cell with NMC 6% graphene and 2% Al_2O_3 (S1) as the cathode, which exhibited improved physical characteristics. The anode material was obtained from another lab and formulated with a composite of silicon carbide (SiC), carbon (C), and tin (Sn). The anode material was mixed with polymeric binders and dispersed in N-methyl-2-pyrrolidone (NMP) to form a homogeneous slurry suitable for electrode fabrication. At the start of charging, the cell voltage was 0.6 V and increased rapidly owing to internal resistance and electrode polarization, reaching 1.5 V after 1 minute (Han et al., 2019). As a result of the constant current flowing through the NMC cathode during the primary charging, the voltage gradually increases, corresponding to the deintercalation of lithium ions from the cathode. During the later charging process, the voltage stabilized at approximately 1.5 V, indicating good compatibility with a stable electrode interphase and adequate ionic conductivity. The average voltage during charging was approximately 1.0546 V, and the median voltage was about 1.1306 V. The charging cycle displayed no sudden voltage drops, indicating stable electrode behavior.

The voltage window of 0.6–1.5 V observed in this study does not represent the intrinsic operating voltage of actual NMC cathodes, which is typically around 3.6–4.2 V (Khan et al., 2025). Instead, it reflects the electrochemical response of the extracted and modified NMC (NMC–graphene–Al_2O_3) under a specific short-duration charging configuration. The measurement was intended as a primary screening to evaluate charge acceptance and electrochemical activity of the modified cathode rather than to determine the full operating voltage window of NMC in conventional Li-ion half-cells.

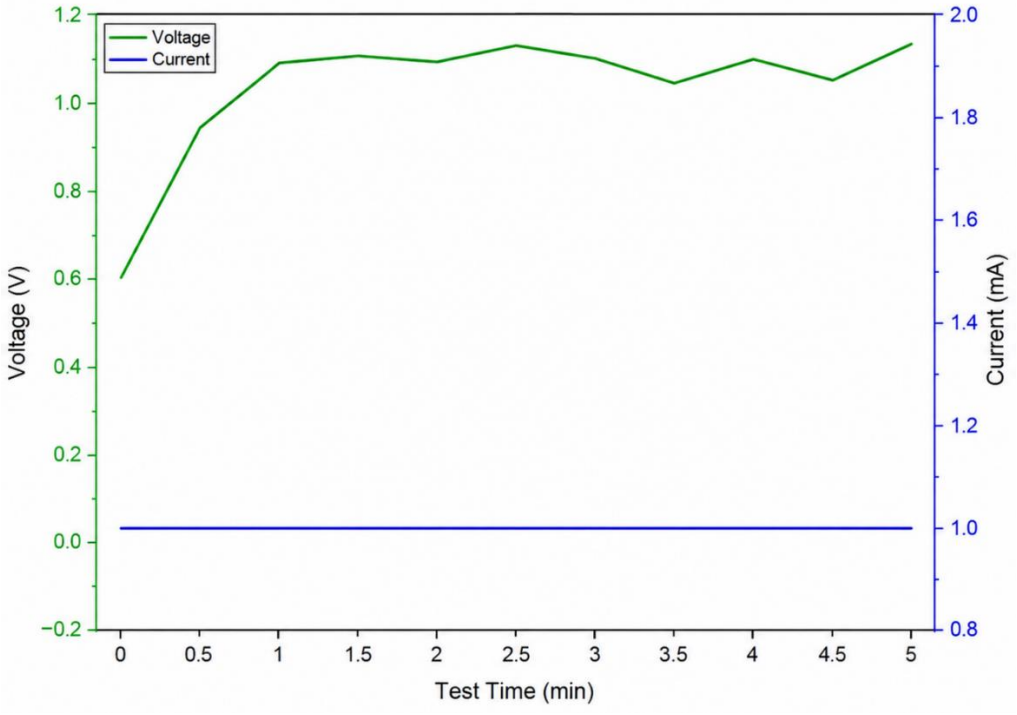


Figure 8. Charging test analysis of the fabricated cell with NMC + 2% Al_2O_3 + 6% graphene cathode.

© 2026 Conscientia Beam. All Rights Reserved.

4. CONCLUSIONS

Our study demonstrated the successful synthesis of multilayered graphene by a two-step pyrolysis method, using waste plastic as a carbon precursor, and its incorporation into a Nickel–Manganese–Cobalt oxide (NMC) cathode with alumina (Al_2O_3) and graphene composites. FESEM analysis revealed graphene nanosheets with overlapping lines or ridges on the surface, stacked randomly. The X-ray diffraction (XRD) spectra exhibited prominent graphene peaks at the (002) and (004) reflections at 26.94° and 55°, respectively. According to Raman spectroscopy, the ID/IG intensity ratio is 1.07, suggesting structural disorder and limited crystalline domain size typical of pyrolysis-derived graphene, and the I_{2D}/I_G ratio is less than 1.0, indicating the multilayer nature of the synthesized material. The FTIR spectrum exhibited the presence of several functional groups, namely hydroxyl (O-H), cyclic nitroxides (N-O), and carbonyl (O=C=O), which can be attributed to mild oxidation of graphene. It loses only 20% of its weight from room temperature to 750 °C, satisfying the requirements for the thermal stability of synthesized graphene. Characterization of the modified NMC cathodes confirmed successful incorporation of graphene and Al_2O_3. Among the investigated compositions, the cathode containing 2.0 wt.% Al_2O_3 and 6.0 wt.% graphene exhibited improved surface morphology and structural stability compared to other formulations. The charging test results for this combination also provide sufficient evidence of the stability of the fabricated electrodes. Overall, the two-step pyrolysis approach provides a sustainable pathway for converting plastic waste into multilayer graphene suitable for cathode modification, highlighting its potential for scalable graphene production and applications in advanced battery systems.

Funding: The authors confirm that no external agencies, institutions, organizations, or sponsors were involved in the support or funding of this study.
Institutional Review Board Statement: This study was conducted by two groups of students as part of their undergraduate thesis and did not require formal IRB approval according to our institutional policy.
Transparency: The authors state that the manuscript is honest, truthful, and transparent, that no key aspects of the investigation have been omitted, and that any differences from the study as planned have been clarified. This study followed all writing ethics.
Competing Interests: The authors declare that they have no competing interests.
Authors' Contributions: All authors contributed equally to the conception and design of the study. All authors have read and agreed to the published version of the manuscript.
Acknowledgment: The authors acknowledge Dhaka University of Engineering & Technology, Gazipur, Bangladesh, for providing scientific and technical support to conduct this research work.

REFERENCES

Ahaliabadeh, Z., Kong, X., Fedorovskaya, E., & Kallio, T. (2022). Extensive comparison of doping and coating strategies for Ni-rich positive electrode materials. *Journal of Power Sources, 540*, 231633. https://doi.org/10.1016/j.jpowsour.2022.231633

Ali, M. O., Islam, E., Abedin, M. Z., Hasan, M., Ali, M. R., Ali, M. J., & Mahmud, S. (2026). Status, pathways and prospects of renewable energy generation from waste streams in Bangladesh: A case study in the major cities. *Energy Reports, 15*, 109226. https://doi.org/10.1016/j.egyr.2026.109226

Ali, M. R., Chowdhury, M. A., Rahman, M. M., Ali, M. O., Mahmud, S., Rana, M. M., & Roy, B. K. (2023). Performance enhancement of lithium-ion battery using modified LiMn2O4 cathode followed by ultrasonic-assisted electrochemically synthesized graphene. *Results in Engineering, 20*, 101578. https://doi.org/10.1016/j.rineng.2023.101578

Argañaraz, M. P. Q., Jori, K., Ramallo-López, J. M., Visintin, A., Requejo, F. G., & Ortiz, M. G. (2025). Enhancement of LiFePO4 cathodic material through incorporation of reduced graphene oxide via a simple two-step procedure. *Journal of Physics and Chemistry of Solids, 196*, 112353. https://doi.org/10.1016/j.jpcs.2024.112353

Ayiania, M., Weiss-Hortala, E., Smith, M., McEwen, J.-S., & Garcia-Perez, M. (2020). Microstructural analysis of nitrogen-doped char by Raman spectroscopy: Raman shift analysis from first principles. *Carbon, 167*, 559-574. https://doi.org/10.1016/j.carbon.2020.05.055

Balandin, A. A., Ghosh, S., Bao, W., Calizo, I., Teweldebrhan, D., Miao, F., & Lau, C. N. (2008). Superior thermal conductivity of single-layer graphene. *Nano Letters, 8*(3), 902-907. https://doi.org/10.1021/nl0731872

© 2026 Conscientia Beam. All Rights Reserved.

Balqis, N., Mohamed Jan, B., Simon Cornelis Metselaar, H., Sidek, A., Kenanakis, G., & Ikram, R. (2023). An overview of recycling wastes into graphene derivatives using microwave synthesis; trends and prospects. *Materials*, *16*(10), 3726. https://doi.org/10.3390/ma16103726

Belbessai, S., Benyoussef, E.-H., Gitzhofer, F., & Abatzoglou, N. (2022). Carbon nanomaterial production using waste plastic pyrolysis over a new catalyst made from mining residues: Effect of plastic type. *Chemical Engineering Journal Advances*, *12*, 100424. https://doi.org/10.1016/j.ceja.2022.100424

Bharti, R. G., & Sharma, R. (2021). Analysis of plastic waste management: Utilization, issues & solutions. *Materials Today: Proceedings*, *45*, 3625-3632.

Biró, L. P., & Lambin, P. (2013). Grain boundaries in graphene grown by chemical vapor deposition. *New Journal of Physics*, *15*(3), 035024. https://doi.org/10.1088/1367-2630/15/3/035024

Blázquez-Moreno, J. M., Morales-Calero, F. J., Cobos-Luque, A., Raya, A. M., Rincón, R., Benítez, A., & Caballero, Á. (2025). Ethanol-derived graphene by microwave plasma torch as efficient cathode for Li-S batteries with ultralong cycle life. *Journal of Power Sources*, *630*, 236173. https://doi.org/10.1016/j.jpowsour.2025.236173

Chen, R. L. B., Sayed, F. N., Banerjee, H., Temprano, I., Wan, J., Morris, A. J., & Grey, C. P. (2025). Identification of the dual roles of Al2O3 coatings on NMC811-cathodes via theory and experiment. *Energy & Environmental Science*, *18*(4), 1879-1900. https://doi.org/10.1039/D4EE03444A

Chen, S., Lin, J., Shi, Q., Cai, Z., Cao, L., Zhu, L., & Yuan, Z. (2020). Nanoscale iron fluoride supported by three-dimensional porous graphene as long-life cathodes for lithium-ion batteries. *Journal of The Electrochemical Society*, *167*(8), 080506. https://doi.org/10.1149/1945-7111/ab88be

Chen, W., Ge, C., Li, J. T., Beckham, J. L., Yuan, Z., Wyss, K. M., . . . Tour, J. M. (2022). Heteroatom-doped flash graphene. *ACS Nano*, *16*(4), 6646-6656. https://doi.org/10.1021/acsnano.2c01136

Chojaa, H., Derouich, A., Zamzoum, O., Mahfoud, S., Taoussi, M., Albalawi, H., . . . Mosaad, M. I. (2023). A novel DPC approach for DFIG-based variable speed wind power systems using DSpace. *IEEE Access*, *11*, 9493-9510. https://doi.org/10.1109/ACCESS.2023.3237511

Derakhshi, M., Daemi, S., Shahini, P., Habibzadeh, A., Mostafavi, E., & Ashkarran, A. A. (2022). Two-dimensional nanomaterials beyond graphene for biomedical applications. *Journal of Functional Biomaterials*, *13*(1), 27. https://doi.org/10.3390/jfb13010027

Dey, S., Veerendra, G. T. N., Babu, P. S. S. A., Manoj, A. V. P., & Nagarjuna, K. (2024). Degradation of plastics waste and its effects on biological ecosystems: A scientific analysis and comprehensive review. *Biomedical Materials & Devices*, *2*(1), 70-112. https://doi.org/10.1007/s44174-023-00085-w

Dhali, S., Karakoti, M., Dandapat, A., & Sahoo, N. G. (2023). Synthesis of graphene from waste plastic and its applications. In C. M. Hussain, A. K. Srivastav, C. S. Tiwary, & J. M. Tour (Eds.), *Graphene extraction from waste: A sustainable synthesis approach for graphene and its derivatives* (pp. 55–76). Cambridge, England: Woodhead Publishing.

Elessawy, N. A., Rafea, M. A., Roushdy, N., Youssef, M. E., & Gouda, M. H. (2023). Development and evaluation of cost-effective and green Bi-functional nickel oxide decorated graphene electrocatalysts for alkaline fuel cells. *Results in Engineering*, *17*, 100871. https://doi.org/10.1016/j.rineng.2022.100871

Fang, W., Zhao, H., Xie, Y., Fang, J., Xu, J., & Chen, Z. (2015). Facile hydrothermal synthesis of VS2/graphene nanocomposites with superior high-rate capability as lithium-ion battery cathodes. *ACS Applied Materials & Interfaces*, *7*(23), 13044-13052. https://doi.org/10.1021/acsami.5b03124

Ferrari, A. C., Meyer, J. C., Scardaci, V., Casiraghi, C., Lazzeri, M., Mauri, F., . . . Geim, A. K. (2006). The Raman fingerprint of graphene. *arXiv preprint cond-mat/0606284*. https://doi.org/10.48550/arXiv.cond-mat/0606284

Garg, K. K., Pandey, S., Kumar, A., Rana, A., Sahoo, N. G., & Singh, R. K. (2022). Graphene nanosheets derived from waste plastic for cost-effective thermoelectric applications. *Results in Materials*, *13*, 100260. https://doi.org/10.1016/j.rinma.2022.100260

Geim, A. K., & Novoselov, K. S. (2007). The rise of graphene. *Nature Materials*, *6*(3), 183-191. https://doi.org/10.1038/nmat1849

© 2026 Conscientia Beam. All Rights Reserved.

Güngör, H., Güler, A., Çoban, A., Güler, M. O., & Akbulut, H. (2018). *Graphene assisted NMC based cathode electrodes with enhanced charge rate and energy storage*. Paper presented at the UCTEA Chamber of Metallurgical and Materials Engineers Training Center Proceedings, Turkey.

Han, B., Paulauskas, T., Key, B., Peebles, C., Park, J. S., Klie, R. F., . . . Dogan, F. (2017). Understanding the role of temperature and cathode composition on interface and bulk: Optimizing aluminum oxide coatings for Li-ion cathodes. *ACS Applied Materials & Interfaces*, *9*(17), 14769-14778. https://doi.org/10.1021/acsami.7b00595

Han, X., Feng, X., Ouyang, M., Lu, L., Li, J., Zheng, Y., & Li, Z. (2019). A comparative study of charging voltage curve analysis and state of health estimation of lithium-ion batteries in electric vehicle. *Automotive Innovation*, *2*(4), 263-275. https://doi.org/10.1007/s42154-019-00080-2

Huang, H., Chen, S., Wee, A. T. S., & Chen, W. (2014). Epitaxial growth of graphene on silicon carbide (SiC), Graphene. In V. Skákalová & A. B. Kaiser (Eds.), *Graphene: Properties, preparation, characterisation and devices* (pp. 3–26). Cambridge, England: Woodhead Publishing.

Itoo, A. M., Vemula, S. L., Gupta, M. T., Giram, M. V., Kumar, S. A., Ghosh, B., & Biswas, S. (2022). Multifunctional graphene oxide nanoparticles for drug delivery in cancer. *Journal of Controlled Release*, *350*, 26-59. https://doi.org/10.1016/j.jconrel.2022.08.011

Ivanov, A. V., Maksimova, N. V., Kamaev, A. O., Malakho, A. P., & Avdeev, V. V. (2018). Influence of intercalation and exfoliation conditions on macrostructure and microstructure of exfoliated graphite. *Materials Letters*, *228*, 403-406. https://doi.org/10.1016/j.matlet.2018.06.072

Jahandari, A. (2023). Microplastics in the urban atmosphere: Sources, occurrences, distribution, and potential health implications. *Journal of Hazardous Materials Advances*, *12*, 100346. https://doi.org/10.1016/j.hazadv.2023.100346

Jekal, S., Kim, C.-G., Kim, J., Kim, H.-Y., Chu, Y.-R., Ra, Y.-H., . . . Yoon, C.-M. (2024). Enhanced electrochemical performance of lithium iron phosphate cathodes using plasma-assisted reduced graphene oxide additives for lithium-ion batteries. *Batteries*, *10*(10), 345. https://doi.org/10.3390/batteries10100345

Jiang, L., Niu, T., Lu, X., Dong, H., Chen, W., Liu, Y., . . . Zhu, D. (2013). Low-temperature, bottom-up synthesis of graphene via a radical-coupling reaction. *Journal of the American Chemical Society*, *135*(24), 9050-9054. https://doi.org/10.1021/ja4031825

Kang, S. B., Jo, Y., Lam, N. H., Truong, N. T. N., Jung, J. H., & Kim, C.-D. (2023). Nitrogen-doped nickel graphene core shell synthesis: Structural, morphological, and chemical composition for planar hybrid solar cells application. *Photonics*, *10*(1), 18. https://doi.org/10.3390/photonics10010018

Khan, M. A., Thatipamula, S., Tresca, L., Xu, L., Trewartha, A., & Onori, S. (2025). High-power lithium-ion battery characterization dataset for stochastic battery modeling. *Scientific Data*, *12*(1), 1506. https://doi.org/10.1038/s41597-025-05725-y

Kim, C.-D., Truong, N. T. N., Pham, V. T. H., Jo, Y., Lee, H.-R., & Park, C. (2019). Conductive electrodes based on Ni–graphite core–shell nanoparticles for heterojunction solar cells. *Materials Chemistry and Physics*, *223*, 557-563. https://doi.org/10.1016/j.matchemphys.2018.11.019

Kumar, N. A., Gambarelli, S., Duclairoir, F., Bidan, G., & Dubois, L. (2013). Synthesis of high quality reduced graphene oxide nanosheets free of paramagnetic metallic impurities. *Journal of Materials Chemistry A*, *1*(8), 2789-2794. https://doi.org/10.1039/C2TA01036D

Kumar, R., Mehta, B. R., Bhatnagar, M., Ravi, S., Mahapatra, S., Salkalachen, S., & Jhawar, P. (2014). Graphene as a transparent conducting and surface field layer in planar Si solar cells. *Nanoscale Research Letters*, *9*(1), 349. https://doi.org/10.1186/1556-276x-9-349

Kumarov, A., Yerkinbekova, Y., Zheng, M., Amin, P., Barbiellini, B., Rezaei, N., . . . Laakso, E. (2025). Plasma-assisted reduced graphene oxide-wrapped Ni-rich cathode materials for Li-ion batteries. *Chemical Engineering Journal*, *525*, 170156. https://doi.org/10.1016/j.cej.2025.170156

Lan, Y., Zondode, M., Deng, H., Yan, J.-A., Ndaw, M., Lisfi, A., . . . Pan, Y.-L. (2018). Basic concepts and recent advances of crystallographic orientation determination of graphene by Raman spectroscopy. *Crystals*, *8*(10), 375. https://doi.org/10.3390/cryst8100375

© 2026 Conscientia Beam. All Rights Reserved.

Lavin-Lopez, M. P., Valverde, J. L., Sanchez-Silva, L., & Romero, A. (2016). Solvent-based exfoliation via sonication of graphitic materials for graphene manufacture. *Industrial & Engineering Chemistry Research*, *55*(4), 845-855. https://doi.org/10.1021/acs.iecr.5b03502

Lee, C., Wei, X., Kysar, J. W., & Hone, J. (2008). Measurement of the elastic properties and intrinsic strength of monolayer graphene. *Science*, *321*(5887), 385-388. https://doi.org/10.1126/science.1157996

Liu, J., Bao, S., & Wang, X. (2022). Applications of graphene-based materials in sensors: A review. *Micromachines*, *13*(2), 184. https://doi.org/10.3390/mi13020184

Llanos, P. S., Ahaliabadeh, Z., Miikkulainen, V., Lahtinen, J., Yao, L., Jiang, H., . . . Kallio, T. M. (2024). High voltage cycling stability of LiF-coated NMC811 electrode. *ACS Applied Materials & Interfaces*, *16*(2), 2216-2230. https://doi.org/10.1021/acsami.3c14394

Loghavi, M. M., Babaiee, M., & Eqra, R. (2023). Al2O3-coated LiNi0.8Co0.15Al0.05O2/graphene composite as a high-performance cathode material for lithium-ion battery. *Main Group Chemistry*, *22*(1), 67-77. https://doi.org/10.3233/MGC-220025

Ma, Y., Cui, P., Gan, B., Ma, Y., & Liang, Y. (2018). Graphene oxide modified LiNi1/3Co1/3Mn1/3O2 as cathode material for lithium ion batteries and its electrochemical performances. *International Journal of Electrochemical Science*, *13*(11), 10440-10453. https://doi.org/10.20964/2018.11.17

Malayeri, M. A., Koohestani, H., & Tajally, M. (2023). Improving the properties of nickel/graphene oxide coated copper plate by changing the electroplating process conditions. *Results in Engineering*, *18*, 101167. https://doi.org/10.1016/j.rineng.2023.101167

Mohanty, D., Dahlberg, K., King, D. M., David, L. A., Sefat, A. S., Wood, D. L., . . . Albano, F. (2016). Modification of Ni-rich FCG NMC and NCA cathodes by atomic layer deposition: Preventing surface phase transitions for high-voltage lithium-ion batteries. *Scientific Reports*, *6*(1), 26532. https://doi.org/10.1038/srep26532

Ojha, A., Samriti, Thakur, S., & Prakash, J. (2023). Graphene family nanomaterials as emerging sole layered nanomaterials for wastewater treatment: Recent developments, potential hazards, prevention and future prospects. *Environmental Advances*, *13*, 100402. https://doi.org/10.1016/j.envadv.2023.100402

Okonkwo, P. C., Emori, W., Uzoma, P. C., Mansir, I. B., Radwan, A. B., Ige, O. O., & Abdullah, A. M. (2022). A review of bipolar plates materials and graphene coating degradation mechanism in proton exchange membrane fuel cell. *International Journal of Energy Research*, *46*(4), 3766-3781. https://doi.org/10.1002/er.7428

Pandey, S., Karakoti, M., Dhali, S., Karki, N., SanthiBhushan, B., Tewari, C., . . . Sahoo, N. G. (2019). Bulk synthesis of graphene nanosheets from plastic waste: An invincible method of solid waste management for better tomorrow. *Waste Management*, *88*, 48-55. https://doi.org/10.1016/j.wasman.2019.03.023

Park, D., Sherrell, P. C., Xie, F., & Ellis, A. V. (2024). Improved lithium-ion battery cathode rate performance via carbon black functionalization. *Journal of Materials Chemistry A*, *12*(8), 4884-4892. https://doi.org/10.1039/D3TA05093A

Ramos, T. M., Christensen, T. B., Bour, A., Almroth, B. C., Kristensen, D. M., Selck, H., & Syberg, K. (2023). A not so circular healthcare economy: A review of challenges with plastic associated chemicals. *TrAC Trends in Analytical Chemistry*, *166*, 117191. https://doi.org/10.1016/j.trac.2023.117191

Ren, S., Xu, X., Hu, K., Tian, W., Duan, X., Yi, J., & Wang, S. (2022). Structure-oriented conversions of plastics to carbon nanomaterials. *Carbon Research*, *1*(1), 15. https://doi.org/10.1007/s44246-022-00016-2

Ronduda, H., Zybert, M., Szczęsna-Chrzan, A., Trzeciak, T., Ostrowski, A., Szymański, D., . . . Marcinek, M. (2020). On the sensitivity of the Ni-rich layered cathode materials for Li-ion batteries to the different calcination conditions. *Nanomaterials*, *10*(10), 2018. https://doi.org/10.3390/nano10102018

Saeed, M., Alshammari, Y., Majeed, S. A., & Al-Nasrallah, E. (2020). Chemical vapour deposition of graphene—synthesis, characterisation, and applications: A review. *Molecules*, *25*(17), 3856. https://doi.org/10.3390/molecules25173856

Saffanah, U., Avis, W., Widiyandari, H., Jumari, A., & Purwanto, A. (2025). Extreme fast charging of lithium-ion batteries using flash graphene additive. *Electrochemistry Communications*, *177*, 107984. https://doi.org/10.1016/j.elecom.2025.107984

Salahdin, O. D., Sayadi, H., Solanki, R., Parra, R. M. R., Al-Thamir, M., Jalil, A. T., . . . Kianfar, E. (2022). Graphene and carbon structures and nanomaterials for energy storage. *Applied Physics A*, *128*(8), 703.

© 2026 Conscientia Beam. All Rights Reserved.

Saleem, H., Haneef, M., & Abbasi, H. Y. (2018). Synthesis route of reduced graphene oxide via thermal reduction of chemically exfoliated graphene oxide. *Materials Chemistry and Physics*, *204*, 1-7. https://doi.org/10.1016/j.matchemphys.2017.10.020

Sanad, M. M. S., Meselhy, N. K., El-Boraey, H. A., & Toghan, A. (2023). Controllable engineering of new ZnAl2O4-decorated LiNi0·8Mn0·1Co0·1O2 cathode materials for high performance lithium-ion batteries. *Journal of Materials Research and Technology*, *23*, 1528-1542. https://doi.org/10.1016/j.jmrt.2023.01.102

Setyawati, R. B., Stulasti, K. N. R., Azinuddin, Y. R., Suci, W. G., Aliwarga, H. K. K., Dyartanti, E. R., & Purwanto, A. (2024). High power and thermal-stable of graphene modified LiNi0.8Mn0.1Co0.1O2 cathode by simple method for fast charging-enable lithium ion battery. *Results in Engineering*, *21*, 101651. https://doi.org/10.1016/j.rineng.2023.101651

Soltani, T., & Lee, B.-K. (2017). A benign ultrasonic route to reduced graphene oxide from pristine graphite. *Journal of Colloid and Interface Science*, *486*, 337-343. https://doi.org/10.1016/j.jcis.2016.09.075

Tan, K. Q., Ahmad, M. A., Da Oh, W., & Low, S. C. (2023). Valorization of hazardous plastic wastes into value-added resources by catalytic pyrolysis-gasification: A review of techno-economic analysis. *Renewable and Sustainable Energy Reviews*, *182*, 113346. https://doi.org/10.1016/j.rser.2023.113346

Tang, B., Guoxin, H., & Gao, H. (2010). Raman spectroscopic characterization of graphene. *Applied Spectroscopy Reviews*, *45*(5), 369-407. https://doi.org/10.1080/05704928.2010.483886

Tarhini, A., & Tehrani-Bagha, A. R. (2023). Advances in preparation methods and conductivity properties of graphene-based polymer composites. *Applied Composite Materials*, *30*(6), 1737-1762. https://doi.org/10.1007/s10443-023-10145-5

Tunca, F. S., Sevinç, A. T., Usta, S., Çetinkaya, T., Akbulut, H., & Tokur, M. (2024). Optimization of NMC cathode inks for cost-effective and eco-friendly screen-printed lithium-ion batteries. *Electrochimica Acta*, *493*, 144429. https://doi.org/10.1016/j.electacta.2024.144429

Velasco, D. L., Díez-Pascual, A. M., & Capilla, P. R. (2022). Application of graphene-related materials in organic solar cells. *Materials*, *15*(3), 1171. https://doi.org/10.3390/ma15031171

Vieira, O., Ribeiro, R. S., De Tuesta, J. L. D., Gomes, H. T., & Silva, A. M. T. (2022). A systematic literature review on the conversion of plastic wastes into valuable 2D graphene-based materials. *Chemical Engineering Journal*, *428*, 131399. https://doi.org/10.1016/j.cej.2021.131399

Whitener, J. K. E., & Sheehan, P. E. (2014). Graphene synthesis. *Diamond and Related Materials*, *46*, 25-34. https://doi.org/10.1016/j.diamond.2014.04.006

Wu, J., Lin, H., Moss, D. J., Loh, K. P., & Jia, B. (2023). Graphene oxide for photonics, electronics and optoelectronics. *Nature Reviews Chemistry*, *7*(3), 162-183. https://doi.org/10.1038/s41570-022-00458-7

Wu, Y., Ye, H., You, C., Zhou, W., Chen, J., Xiao, W., . . . Yuan, Z. (2022). Construction of functionalized graphene separation membranes and their latest progress in water purification. *Separation and Purification Technology*, *285*, 120301. https://doi.org/10.1016/j.seppur.2021.120301

Yerkinbekova, Y., Kumarov, A., Tatykayev, B., Mentbayeva, A., Repo, E., & Laakso, E. (2025). Ni-rich cathode materials with concentration gradients for high-energy and safe lithium-ion batteries: A comprehensive review. *Journal of Power Sources*, *626*, 235686. https://doi.org/10.1016/j.jpowsour.2024.235686

Zhang, F., Liang, Y., Ye, Z., Deng, L., Guo, Y., Qiu, P., . . . Zhang, L. (2024). Enhanced electrochemical performance of nanoscale single crystal NMC811 modification by coating LiNbO3. *Chinese Chemical Letters*, *35*(5), 108655. https://doi.org/10.1016/j.cclet.2023.108655

Zhou, M., Tang, J., Cheng, Q., Xu, G., Cui, P., & Qin, L.-C. (2013). Few-layer graphene obtained by electrochemical exfoliation of graphite cathode. *Chemical Physics Letters*, *572*, 61-65. https://doi.org/10.1016/j.cplett.2013.04.013

Views and opinions expressed in this article are the views and opinions of the author(s), International Journal of Sustainable Energy and Environmental Research shall not be responsible or answerable for any loss, damage or liability etc. caused in relation to/arising out of the use of the content.

© 2026 Conscientia Beam. All Rights Reserved.